Published in final edited form as:
J Nucl Med. 2013 April ; 54(4): 609–615. doi:10.2967/jnumed.112.108092.

Quantitative Positron Emission Tomography Imaging Detects Early Metabolic Remodeling in a Mouse Model of Pressure Overload Left Ventricular Hypertrophy in vivo

Min Zhong[1,2,#], **Clayton E. Alonso**[2], **Heinrich Taegtmeyer**[3], and **Bijoy K. Kundu**[2,4,*]

[1]Department of Physics, University of Virginia, Charlottesville, VA, 22903

[2]Department of Radiology and Medical Imaging, University of Virginia, Charlottesville, VA 22908

[3]Department of Internal Medicine, Division of Cardiology, University of Texas Medical School at Houston, Houston, TX 77030

[4]Cardiovascular Research Center, University of Virginia, Charlottesville, VA 22908

Abstract

We proposed that metabolic remodeling in the form of increased myocardial glucose analogue 2-[^{18}F] fluoro-2deoxy-D-glucose (FDG) uptake precedes and triggers the onset of severe contractile dysfunction in pressure overload left ventricular hypertrophy (LVH) *in vivo*. To test this hypothesis we used a mouse model of transverse aortic constriction (TAC) together with Positron Emission Tomography (PET) and assessed serial changes in cardiac metabolism and function over 7 days.

Methods—PET scans of 16 C57BL/6 male mice were performed using a microPET scanner under sevofluorane anesthesia. A 10-minute transmission scan was followed by a 60-minute dynamic FDG-PET scan with cardiac and respiratory gating. Blood glucose levels were measured before and after the emission scan. Transverse aortic constriction (TAC) and sham surgeries were performed after baseline imaging. Osmotic mini-pumps containing either propranolol (5 mg/kg/day) or vehicle alone were implanted subcutaneously at the end of surgery. Subsequent scans were taken at days 1 and 7 after surgery. A compartment model, in which the blood input function with spill-over and partial volume corrections and the metabolic rate constants in a 3-compartment model are simultaneously estimated, was used to determine the net myocardial FDG influx constant, Ki. The rate of myocardial glucose use, rMGU, was also computed. Estimations of the ejection fractions (EF) were based on the high resolution gated PET images

Results—Mice undergoing TAC surgery exhibited an increase in the Ki (580%) and glucose usage the day after surgery indicating early adaptive response. On day 7 the EF had decreased by 24% indicating a maladaptive response. Average Ki increases were not linearly associated with increases in rMGU. Ki exceeded rMGU by 29% in the TAC mice. TAC Mice treated with propranolol attenuated rate of FDG uptake, diminished mismatch between Ki and rMGU (9%) and rescued cardiac function.

Conclusions—Metabolic maladaptation precedes the onset of severe contractile dysfunction. Both are prevented by treatment with propranolol. Early detection of metabolic remodeling may offer a metabolic target for modulation of hypertrophy.

[*]Corresponding Author: Bijoy K. Kundu, PhD, Assistant Professor, Department of Radiology and Medical Imaging, Cardiovascular Research Center, University of Virginia, Charlottesville, VA 22908, bkk5a@virginia.edu, Phone: 434-924-0284, Fax: 434-924-9435.
[#]**First Author:** Min Zhong, MA, PhD Student, Department of Physics, Radiology and Medical Imaging, University of Virginia, Charlottesville, VA 22908, mz3bs@virginia.edu, Phone: 434-466-3537, Fax: 434-924-9435

Keywords

FDG-PET; Glucose Metabolism in Heart; Left Ventricular Ejection Fraction; Left Ventricular Hypertrophy

INTRODUCTION

Myocardial hypertrophy is considered initially an adaptive response to stress. When stress is sustained, however, hypertrophy becomes maladaptive. Both functional and structural changes are accompanied by changes in energy substrate metabolism. A hallmark finding in myocardial hypertrophy is a shift away from fatty-acid to glucose oxidation (1). Based on earlier work *ex vivo*, we have proposed that this metabolic remodeling precedes and triggers LV structural and functional remodeling in pressure overload left ventricular hypertrophy (LVH) and induces the fetal gene program (2–4). However, this hypothesis has never been evaluated *in vivo*. For this purpose we used the mouse model of left ventricular pressure overload after transverse aortic constriction (TAC) as a clinically relevant model to assess metabolism and function of the heart subjected to pressure overload using 2-[^{18}F] fluoro-2deoxy-D-glucose (FDG) Positron Emission Tomography (PET) imaging.

A compartmental modeling technique was used to analyze images obtained dynamically to compute rate of myocardial FDG uptake and utilization. The quantification of these rates has been limited by two important factors: a) the limited spatial resolution of the small animal PET scanners (5, 6) leading to partial volume (PV) effects, and b) the spill-over (SP) of radioactivity from the blood pool (BP) to the myocardium and vice-versa. A major shortcoming of the image-derived blood input function (IDIF) method is that it is susceptible to SP and PV effects (7).

In this study, a compartment model corrected blood input function (MCBIF) was optimized, wherein the blood input function with SP and PV corrections and the metabolic rate constants in a 3-compartment model were simultaneously estimated from OSEM-MAP cardiac and respiratory gated PET images with attenuation correction (8). Left ventricular ejection fraction (LVEF) was also measured using high resolution gated PET images, which enabled us to perform a side-by-side comparison of cardiac metabolism, and LV function.

MATERIALS AND METHODS

Animal Model

Sixteen adult C57BL/6 male mice (9–10 weeks of age) obtained from Charles River were imaged at baseline using a microPET Focus-F120 scanner (Siemens, Inc.) under sevofluorane anesthesia (9). A subset of these mice (n=11) were subjected to a transverse aortic constriction (TAC) surgical procedure to induce pressure-overload hypertrophy (10). Briefly, mice were anesthetized with isoflurane and intubated for ventilation. A thoracotomy was performed and a 7-0 silk suture was tied around the transverse aorta between the proximal and distal carotid arteries against a 27-gauge needle, after which, the needle was removed. Osmotic mini-pumps containing either propranolol (5 mg/kg/day) obtained from Sigma Aldrich Inc. (n=6) or vehicle alone (n=5) were implanted subcutaneously at the end of surgery. In addition, five sham-operated animals were subjected to the same surgical protocol, without tying off the suture. Before and after surgery all mice were kept in a 12 hrs light/12 hrs dark cycle environment. Prior to imaging, animals were fasted (11) overnight with only access to water.

PET scans were performed between 9 a.m. and 5 p.m. on anesthetized animals. All experiments were performed in compliance with the Guide for the Care and Use of Laboratory Animals, published by the National Institutes of Health and was conducted under protocols approved by the Institutional Animal Care and Use Committee at the University of Virginia.

MicroPET Imaging

PET imaging for measuring myocardial FDG uptake and glucose utilization was carried out using ^{18}F-FDG in the sham, TAC and TAC treated with propranolol mice as follows: Following the insertion of a tail-vein catheter, ECG surface electrodes (Blue Sensor, Ambu Inc., Glen Burnie, MD) were placed on both forepaws and the left hindpaw and a pneumatic respiratory pillow was placed on the animal's chest. 60 minute dynamic PET scan was performed under 2.5% sevoflurane anesthesia in oxygen (9), where data acquisition was initiated a few seconds before the slow administration of about 800 μCi FDG over 30–60 seconds via the catheter. Small Animal Instruments, Inc., model 1025L for PET was used for continuously monitoring heart rate, respiration, and core body temperature (rectal probe). Cardiac gate signals were generated at the end-expiration phase of the respiratory cycle to time-stamp the PET scanner data for subsequent retrospective reordering into heart and respiratory-cycle based time-bins (12). Transmission scan using Co57 point source was done for attenuation correction prior to FDG administration. The list mode data sorted into 23 time bins (11 × 8 s, 1 × 12 s, 2 × 60s, 1 × 180 s, and 8 × 400 s) and 3 gates (hence referred to as gated) were reconstructed using OSEM-MAP algorithm (13, 14) with attenuation correction. For comparison the data were also reconstructed using Filtered Back Projection (FBP) algorithm (ramp filter cutoff at the Nyquist frequency) with the same spatial resolution without gating. The images were corrected for radioactive decay, random coincidences and dead-time losses using the microPET Manager (Siemens Inc.). Regions of interest (ROI) in the region corresponding to the LV blood pool (LVBP) and the myocardium were drawn in the last frame and the last gate of the dynamic image data and time activity curves for the LVBP and the myocardium were generated for the whole scan duration of 60 minutes. Blood samples were also collected at around 43 and 56 minutes post FDG administration from the tail vein to validate the MCBIF. Three blood samples before and 3 blood samples after the PET scan were drawn by a tail-vein nick to measure blood glucose levels using a glucometer (Accu-Chek, Roche). The average of these blood glucose readings were used to compute the rate of myocardial glucose utilization (rMGU).

A compartment model corrected blood input function (MCBIF) (8, 15) was optimized in this manuscript (see below), which is based on simultaneous estimation of the blood input function with SP and PV corrections and the metabolic rate constants. The formalism for MCBIF was utilized to measure the net myocardial FDG influx, Ki and hence glucose utilization, rMGU, in the sham, TAC, and TAC treated with propranolol mice *in vivo*.

End-systolic volumes (ESV) and end-diastolic volumes (EDV) were also measured by drawing ROIs at the end-systolic and end-diastolic phases of the heart cycle over multiple slices covering the whole heart from the apex to the base. The volumes obtained in each phase over multiple slices were summed to obtain net ESV and EDV in micro liters (μl). The LVEF was measured by: (EDV-ESV)/(EDV) × 100 %.

Compartment Model Corrected Blood Input Function (MCBIF)

Based on the 3-compartment FDG model (Fig. 1), the differential equations for FDG kinetics can be written as follows (16):

$$dC_e/dt = K_1 C_p(t) - (k_2+k_3)C_e(t) + k_4 C_m(t) \quad (1)$$

$$dC_m/dt = k_3 C_e(t) - k_4 C_m(t) \quad (2)$$

where, the 3 compartments are 1) $C_p(t)$ is the FDG concentration in the blood compartment, 2) $C_e(t)$ is the concentration of FDG in the interstitial and cellular spaces and 3) $C_m(t)$ is the FDG concentration within the cell of the phosphorylated FDG-6-Phosphate. K_1 and k_2 are the forward rate constant and reverse rate constant respectively between the first 2 compartments. k_3 and k_4 are the rates of phosphorylation and de-phosphorylation between compartments 2 and 3. $C_e(t)$ and $C_m(t)$ can be solved in terms of $C_p(t)$ and the rate constants, K_1–k_4,

$$C_T(t) = \frac{K_1}{a_1 - a_2} \cdot [(k_3+k_4-a_1)e^{-a_1 t} + (a_2-k_3-k_4)e^{-a_2 t}] \otimes C_p(t), \quad (3)$$

where,

$$a_{2,1} = 1/2(k_2+k_3+k_4 \pm \sqrt{(k_2+k_3+k_4)^2 - 4k_2k_4}), \quad (4)$$

and

$$C_T(t) = C_e(t) + C_m(t), \quad (5)$$

is the net myocardium tissue concentration (Fig. 1). Assuming the rate of de-phosphorylation, $k_4 = 0$, the net myocardial FDG influx constant, Ki, can be written as

$$Ki = K_1 \frac{k_3}{(k_2+k_3)}. \quad (6)$$

Ideally, when a region of interest is drawn within the cavity of the left ventricle, the tissue time-activity curve would equal the whole-blood TAC C_P. However, due to SP and PV effects, the model equation for an image-derived time activity curve from the blood pool can be written in terms of fraction of the tissue concentration in the blood compartment and partial recovery of radioactivity concentration from the blood as:

$$Model_{IDIF,i} = \frac{\int_{t_b^i}^{t_e^i} [S_{mb}(C_T(t)) + r_b C_p] dt}{t_e^i - t_b^i}, \quad (7)$$

and similarly for the myocardium tissue, one can write the model equation as:

$$Model_{myo,i} = \frac{\int_{t_b^i}^{t_e^i} [r_m C_T(t) + S_{bm} C_p] dt}{t_e^i - t_b^i}, \quad (8)$$

where, r_m, r_b, are the recovery coefficients (accounting for PV effect) for the myocardium and blood pool respectively. S_{bm}, S_{mb} are the SP coefficients from the blood pool to the myocardium and vice versa respectively. t_b^i *and* t_e^i are the beginning and end times for a single frame in a dynamic PET scan. The model equation for the blood input function can be written as (17):

$$C_p(t)=(A_1(t-\tau)-A_2-A_3)e^{L_1(t-\tau)}+A_2e^{L_2(t-\tau)}+A_3e^{L_3(t-\tau)}, \quad (9)$$

where, each of the terms determines the amplitude, shape and wash-out of the tracer over time. Substituting equations (3) and (9) in equations (7) and (8), the model equations can be optimized to the blood (PET_{IDIF}) and tissue (PET_{myo}) time activity curves obtained from OSEM-MAP cardiac and respiratory gated PET images with attenuation correction as indicated below:

$$O(p)=\sum_{i=1}^{n}[(Model_{IDIF,i}-PET_{IDF,i})^2+(Model_{myo,i}-PET_{myo,i})^2]. \quad (10)$$

The optimization was performed by minimizing the objective function (eq. 10) in the MATLAB programming environment using the function “fmincon”, which is based on an interior-reflective Newton method. The initial guesses and bounds for the PV averaging coefficients (r_m, r_b) are determined beforehand by performing phantom experiments (13). We have kept the bounds for all the kinetic parameters (K_1–k_4) and SP factors (S_{bm}, S_{mb}) open between 0 and 1. As for the input function, one side of the bounds is determined by the distribution of the input function (A_1, A_2, $A_3>0$ *and* L_1, L_2, $L_3<0$) while the other side is wide open. Optimization of equation 10 results in simultaneous estimation of the blood input function, equation 9, and compartment model parameters K_1–k_4 and hence Ki along with the SP and PV coefficients (S_{mb}, r_b, S_{bm}, r_m), without the need for any blood sampling. Simultaneous estimation results in the blood input function, equation 9, to be free of SP contamination and PV corrected in a 3-compartment model. The rate of myocardial glucose utilization can then be computed as:

$$rMGU=K_i[Glu]/LC, \quad (11)$$

in μmoles/g/min,

where, [Glu] is the average non-radioactive blood glucose levels measured using a glucometer and LC is the lumped constant. The lumped constant corrects the difference of affinity between glucose and FDG to glucose transporters and the phosphorylating system. In recent years the value of the lumped constant has been questioned, and it is uncertain which value should be used (18–21). In the 3-compartment model of glucose transfer into cells, the lumped constant is a function of the correlation between the net and the unidirectional rates of uptake of glucose and glucose tracers such as FDG. For sake of simplicity, we like many investigators, have used LC =1 (22, 23).

Statistical Analysis

Statistical analysis was performed using SigmaStat 3.0 (SPSS, Inc, Chicago, IL). Mean values of Ki, [Glu], rMGU and LVEF were calculated with standard error. Two way repeated measures analysis of variance (ANOVA) and Holm-Sidak post hoc test were used to compare mean values in the sham, TAC and TAC treated with propranolol groups at different time points. A p value of less than 0.05 was considered as statistically significant.

RESULTS

Quantitative Accuracy of MCBIF Applied to IDIF from OSEM-MAP Gated Images

Representative IDIF's obtained from OSEM-MAP gated images (line with open squares) and from FBP un-gated images (line with open circles) with attenuation correction are shown in Fig. 2A. MCBIF applied to IDIF obtained from OSEM-MAP gated (line with solid squares) and FBP un-gated images (line with solid circles) are also shown in the figure. The venous blood samples at 43 and 56 minutes are shown for comparison (open triangles). MCBIF applied to the IDIF obtained from high resolution gated images correctly accounted for the wash-out dynamics of FDG from the blood, when compared to the late venous blood samples. Fig. 2B shows MCBIF estimation during the first 5 minutes of the scan, indicating improved PV recovery when applied to IDIF obtained from OSEM-MAP gated images as compared to that obtained from un-gated FBP images.

A residual plot of MCBIF applied to high resolution gated images, when compared to the 2 late venous blood samples obtained from n=6 control mice, is shown in Fig. 3. The analysis revealed an average difference of 0.017 MBq/cc. The precision (standard deviation of differences) was 0.13 MBq/cc. The figure also shows the analysis obtained from FBP un-gated images. The plot indicated an average difference and precision to be 0.28 MBq/cc and 0.33 MBq/cc respectively obtained from the FBP un-gated data set. The residual plot exhibits the quantitative accuracy and repetitive behavior of MCBIF when applied to OSEM-MAP gated images.

Metabolic Remodeling in LVH in Mice In Vivo

Fig. 4 shows representative gated transverse PET images at the last time bin for sham, TAC and TAC treated with propranolol mice at baseline, day 1 and day 7 post surgery. All scans are from the same animals. The images indicate an enlargement in the LV cavity over a period of 7 days in the TAC mice. The images also show an increase in FDG uptake in the TAC mice starting at day 1 indicative of metabolic adaptation in pressure overload LVH.

The measured rate of myocardial FDG uptake, Ki (ml/g/min), for the mice in the 3 categories are shown in Fig. 5A over a period of 7 days. The plot shows increased myocardial FDG uptake at day 1 post TAC surgery by 580% indicating an adaptive response with preserved LVEF (Fig. 5B). Ki increased further at day 7 with a drop in function by 24%. The blood glucose levels and rate of myocardial glucose utilization (rMGU) are also shown in Figs. 6A–B for the 3 categories over a period of 7 days. We observe a drop in the blood glucose levels at day 1 for the sham, TAC and TAC mice treated with propranolol. Mice treated with propranolol show an elevation in blood glucose levels at day 7 significantly different from day 1 and comparable to shams or mice at baseline. The TAC mice exhibit an insignificant increase in the blood glucose levels between day 1 and day 7 (Fig. 6A). The rMGU (Fig. 6B) did not increase linearly with Ki. Rather, rMGU increased at a much slower rate than Ki, thereby resulting in a mismatch of 29% between Ki and rMGU in the TAC mice (Fig. 7). On the other hand, early treatment with propranolol (24) targeting metabolic alterations attenuated rate of myocardial FDG uptake (Fig. 5A), reduced mismatch between Ki and rMGU to 9% and rescued cardiac function (Fig. 5B). The metabolic changes and cardiac function in the TAC mice treated with propranolol were comparable to the shams. The *in vivo* imaging results suggest that early metabolic remodeling may precede and trigger the onset of severe contractile dysfunction in LVH in mice.

DISCUSSION

In the normal heart fatty acid oxidation is the predominant source (60–90%) of ATP, with glucose oxidation and lactate contributing the rest (25). Stress on the myocardium, such as biomechanical stress from pressure overload, changes normal myocardial substrate metabolism. In the case of pressure-overload induced hypertrophy the prevailing notion is that alterations in energy substrate metabolism adversely affect the response to myocardial ischemic stresses and contribute to contractile dysfunction. Specifically, in the hypertrophic heart there is a shift away from fatty acid oxidation towards glucose metabolism (1). At least initially, this metabolic remodeling may be considered as adaptive, most likely because glucose oxidation yields more ATP per atom of oxygen (2). With time, however, the adaptive response becomes maladaptive as this shift in metabolism does not increase ATP production commensurate with the increased demand for energy by the heart.

Recently we have proposed a requirement for hexose 6-phosphate in mTOR signaling, and cardiac growth (26). However, in the setting of insulin resistance, an oversupply of substrate (glucose) may “starve the heart in the midst of plenty” (27). The hypothesis, however, has never been tested serially *in vivo* due to the limited availability of technologies for studying complex metabolic parameters and LV function. It is tempting to speculate that strategies to improve myocardial substrate utilization and to improve metabolic flexibility (3, 28) in the hypertrophic heart may improve contractile performance and prevent the onset of heart failure.

During acute pressure overload and inotropic stimulation (29), glucose oxidation is increased, but it is not yet completely clear how glucose uptake is related to LV function during pressure overload LVH. Studies using Single Photon Emission Computed Tomography (SPECT) imaging have demonstrated that the metabolic switch can be measured in both small animals and human beings (30, 31). However, a serial study on the temporal relationship between glucose uptake and cardiac function *in vivo* in mice using PET has not been done. We demonstrated that MCBIF applied to an IDIF obtained from high resolution gated images with less severe SP and PV effects is quantitative and also repetitive as compared to that obtained from low resolution un-gated images (15). The results of our present study support the hypothesis that increase in glucose metabolism in the form of increased FDG uptake precedes and triggers the onset of severe dysfunction of the heart in LVH. This is an important point, since early detection of metabolic remodeling may lead to early intervention targeting metabolic changes to prevent the onset of severe contractile dysfunction and improve patient outcomes clinically. We also observe that early treatment with propranolol attenuated myocardial glucose uptake and rescued cardiac function *in vivo*. Thus, metabolic imaging with FDG-PET may provide an early indication of a beneficial effect of a therapy, which may provide a platform for aggressive treatment strategies to improve outcomes clinically.

Dietary conditions affect FDG PET imaging studies (32). Some clinical studies use glucose load conditions without fasting to obtain higher quality images. On the other hand, fasting can produce similar quality images. Because we are interested in FDG dynamics, a reasonable contrast between the blood pool and the myocardial tissue enables us to draw ROI’s and determine rate of myocardial FDG influx with SP and PV corrections. Moreover, performing glucose clamps in mice is challenging in addition to the TAC surgery, so we resort to overnight fasting for our FDG PET scans in order to achieve uniform metabolic conditions to obtain Ki, and rMGU.

The lumped constant, LC, is an important parameter in the determination of the rMGU in a dynamic PET scan. This value may vary, depending upon plasma substrate and hormonal

conditions. Many authors have used a constant value of LC to compute MGU in humans with T2D (33). Botker et al. (34) proposed that LC is a function of rates of FDG transport and phosphorylation and applied the method to assess MGU in humans with ischemic cardiomyopathy (35). In a study by Herrero et al (36), a constant value of LC was used for assessing myocardial glucose uptake for FDG PET studies in dogs. However, they also observe that the correlation between Fick derived and PET derived rMGU has lower correlation with variable LC. The correlation coefficient does not differ after correcting for LC=0.67 for FDG PET studies. They also observe that using variable LC leads to significant underestimation of rMGU in large animals. In the current work, we used LC=1 as we did not measure this constant and there is no consensus on how to deal with this issue. The concerns expressed earlier by Botker et al (34) do not apply because here the metabolic conditions were the same for all animals and in steady state. Nevertheless, further studies need to be done to characterize LC in small animal PET imaging of the heart.

Our study is not without limitations. First, FDG can only be considered as a surrogate marker for glucose metabolism. While FDG indirectly assesses glucose transport and phosphorylation the tracer analog is subjected to changes in the lumped constant (18). Secondly, although clinically relevant, the acute nature of the model may be a limitation in evaluating the hypothesis of metabolic remodeling precede and trigger cardiac dysfunction in LVH. The slowly progressive Dahl salt sensitive hypertensive rat model may be more relevant to evaluate metabolic and functional changes in the heart, *in vivo*, but the costs for a study like the present one would be prohibitive (37). Using the one-kidney, one-clip rabbit model of hypertension we have already shown by invasive measurements that metabolic remodeling of the heart precedes hypertrophy (2). Third, we have not considered any possible differences in plasma substrate or hormone levels, although all scans were obtained under the same conditions and errors would be systematic errors.

CONCLUSIONS

Non-invasive serial imaging of the heart subjected to pressure overload hypertrophy using PET supports the hypothesis that changes in glucose analogue FDG metabolism precedes and triggers the onset of severe cardiac dysfunction in LVH. We found that enhanced uptake of FDG by the myocardium in mice subjected to pressure overload hypertrophy precedes and possibly triggers the onset of contractile dysfunction. Early intervention with a standard of care treatment prevented maladaptive response and rescued cardiac function. We speculate that early detection of metabolic remodeling may offer a metabolic target for modulation of hypertrophy.

Acknowledgments

This work was supported by grants from the US Public Health Service HL 102627 (to BKK) and HL 61483 (to HT). We thank Barbara Thornhill for performing the animal surgeries and Gina Wimer for the tail-vein injections during the course of the study.

Reference List

1. Bishop SP, Altschuld RA. Increased glycolytic metabolism in cardiac hypertrophy and congestive failure. Am J Physiol. 1970; 218:153–159. [PubMed: 4243400]
2. Taegtmeyer H, Overturf ML. Effects of moderate hypertension on cardiac function and metabolism in the rabbit. Hypertension. 1988; 11:416–426. [PubMed: 3366475]
3. Taegtmeyer H, Golfman L, Sharma S, et al. Linking gene expression to function: Metabolic flexibility in the normal and diseased heart. Ann N Y Acad Sci. 2004; 1015:202–213. [PubMed: 15201161]

4. Taegtmeyer H, Sen S, Vela D. Return to the fetal gene program: a suggested metabolic link to gene expression in the heart. Ann N Y Acad Sci. 2010; 1188:191–198. [PubMed: 20201903]
5. Laforest R, Longford D, Siegel S, et al. Performance evaluation of the microPET (R) - FOCUS-F120. IEEE Trans Nucl Sci. 2007; 54:42–49.
6. Tai YC, Chatziioannou AF, Yang Y, et al. MicroPET II: design, development and initial performance of an improved microPET scanner for small-animal imaging. Phys Med Biol. 2003; 48:1519–1537. [PubMed: 12817935]
7. Laforest R, Sharp TL, Engelbach JA, et al. Measurement of input functions in rodents: challenges and solutions. Nucl Med Biol. 2005; 32:679–685. [PubMed: 16243642]
8. Zhong M, Locke LW, Kundu BK. Compartment model corrected blood input function estimate improves with iterative image reconstruction algorithm and cardiac gating [abstract]. J Nucl Med. 2011; 52:2104.
9. Flores JE, McFarland LM, Vanderbilt A, et al. The effects of anesthetic agent and carrier gas on blood glucose and tissue uptake in mice undergoing dynamic FDG-PET imaging: sevoflurane and isoflurane compared in air and in oxygen. Mol Imaging Biol. 2008; 10:192–200. [PubMed: 18516648]
10. Liao YL, Ishikura F, Beppu S, et al. Echocardiographic assessment of LV hypertrophy and function in aortic-banded mice: necropsy validation. Am J Physiol Heart Circ Physiol. 2002; 282:H1703–H1708. [PubMed: 11959634]
11. Lee KH, Ko BH, Paik JY, et al. Effects of anesthetic agents and fasting duration on F-18-FDG biodistribution and insulin levels in tumor-bearing mice. J Nucl Med. 2005; 46:1531–1536. [PubMed: 16157537]
12. Yang Y, Rendig S, Siegel S, et al. Cardiac PET imaging in mice with simultaneous cardiac and respiratory gating. Phys Med Biol. 2005; 50:2979–2989. [PubMed: 15972975]
13. Locke LW, Berr SS, Kundu BK. Image-derived input function from cardiac gated maximum a posteriori reconstructed PET images in mice. Mol Imaging Biol. 2011; 13:342–347. [PubMed: 20521133]
14. Qi JY, Leahy RM, Cherry SR, et al. High-resolution 3D Bayesian image reconstruction using the microPET small-animal scanner. Phys Med Biol. 1998; 43:1001–1013. [PubMed: 9572523]
15. Fang YH, Muzic RF Jr. Spillover and partial-volume correction for image-derived input functions for small-animal 18F-FDG PET studies. J Nucl Med. 2008; 49:606–614. [PubMed: 18344438]
16. Krivokapich J, Huang SC, Phelps ME, Barrio JR, Watanabe CR, Selin CE, Shine KI. Estimation of rabbit myocardial metabolic rate for glucose using fluorodeoxyglucose. Am J Physiol. 1982 Dec; 243(6):H884–H895. [PubMed: 7149043]
17. Feng D, Huang SC, Wang X. Models for computer simulation studies of input functions for tracer kinetic modeling with positron emission tomography. Int J Biomed Comp. 1993; 32:95–110.
18. Hariharan R, Bray M, Ganim R, et al. Fundamental limitations of [18F]2-deoxy-2-fluoro-D-glucose for assessing myocardial glucose uptake. Circulation. 1995; 91:2435–2444. [PubMed: 7729031]
19. Botker HE, Bottcher M, Schmitz O, et al. Glucose uptake and lumped constant variability in normal human hearts determined with [F-18]fluorodeoxyglucose. J Nucl Cardiol. 1997; 4:125–132. [PubMed: 9115064]
20. Ng CK, Holden JE, Degrado TR, et al. Sensitivity of myocardial fluorodeoxyglucose lumped constant to glucose and insulin. Am J Physiol. 1991; 260:H593–H603. [PubMed: 1996702]
21. Hashimoto, Katsuji. Lumped constant for deoxyglucose is decreased when myocardial glucose uptake is enhanced. Am J Physiol Heart Circ Physiol. 1999; 276:129–133.
22. Shoghi KI, Gropler RJ, Sharp T, et al. Time course of alterations in myocardial glucose utilization in the Zucker diabetic fatty rat with correlation to gene expression of glucose transporters: a small-animal PET investigation. J Nucl Med. 2008; 49:1320–1327. [PubMed: 18632819]
23. Shoghi KI, Finck BN, Schechtman KB, et al. In vivo metabolic phenotyping of myocardial substrate metabolism in rodents: differential efficacy of metformin and rosiglitazone monotherapy. Circ Cardiovasc Imaging. 2009; 2:373–381. [PubMed: 19808625]

24. Wallhaus TR, Taylor M, Degrado TR, et al. Myocardial free fatty acid and glucose use after carvedilol treatment in patients with congestive heart failure. Circulation. 2001; 103:2441–2446. [PubMed: 11369683]
25. Taegtmeyer H, Hems R, Krebs HA. Utilization of energy-providing substrates in the isolated working rat heart. Biochem J. 1980; 186:701–711. [PubMed: 6994712]
26. Sharma S, Guthrie PH, Chan SS, et al. Glucose phosphorylation is required for insulin-dependent mTOR signalling in the heart. Cardiovasc Res. 2007; 76:71–80. [PubMed: 17553476]
27. Taegtmeyer H. Glucose for the heart: too much of a good thing? J Am Coll Cardiol. 2005; 46(1): 49–50. [PubMed: 15992634]
28. Taegtmeyer H, Dilsizian V. Imaging myocardial metabolism and ischemic memory. Nat Clin Pract Cardiovasc Med. 2008; 5 (Suppl 2):S42–S48. [PubMed: 18641606]
29. Goodwin GW, Taylor CS, Taegtmeyer H. Regulation of energy metabolism of the heart during acute increase in heart work. J Biol Chem. 1998; 273:29530–29539. [PubMed: 9792661]
30. Mochizuki T, Tsukamoto E, Ono T, et al. Sequential change of BMIPP uptake with age in spontaneously hypertensive rat model. Ann Nucl Med. 1997; 11:299–306. [PubMed: 9460521]
31. de las Fuentes L, Herrero P, Peterson LR, et al. Myocardial fatty acid metabolism: independent predictor of left ventricular mass in hypertensive heart disease. Hypertension. 2003; 41:83–87. [PubMed: 12511534]
32. Wong KP, Sha W, Zhang X, Huang SC. Effects of administration route, dietary condition, and blood glucose level on kinetics and uptake of 18F-FDG in mice. J Nucl Med. 2011; 52:800–807. [PubMed: 21498533]
33. Yokoyama I, Inoue Y, Moritan T, et al. Myocardial glucose utilisation in type II diabetes mellitus patients treated with sulphonylurea drugs. Eur J Nucl Med Mol Imaging. 2006; 33:703–708. [PubMed: 16528523]
34. Botker HE, Goodwin GW, Holden JE, et al. Myocardial glucose uptake measured with fluorodeoxyglucose: a proposed method to account for variable lumped constants. J Nucl Med. 1999; 40:1186–1196. [PubMed: 10405141]
35. Wiggers H, Bottcher M, Nielsen TT, et al. Measurement of myocardial glucose uptake in patients with ischemic cardiomyopathy: application of a new quantitative method using regional tracer kinetic information. J Nucl Med. 1999; 40:1292–1300. [PubMed: 10450680]
36. Herrero P, Sharp TL, Dence C, et al. Comparison of 1-(11)C-glucose and (18)F-FDG for quantifying myocardial glucose use with PET. J Nucl Med. 2002; 43:1530–1541. [PubMed: 12411556]
37. Nakamoto M, Ohya Y, Shinzato T, et al. Pioglitazone, a thiazolidinedione derivative, attenuates left ventricular hypertrophy and fibrosis in salt-sensitive hypertension. Hypertension Res. 2008; 31:353–361.

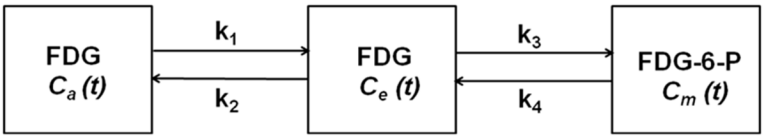

Figure 1. Three compartment FDG model

Block diagram indicating the rate constants, K_1–k_4, between the 3 compartments of the FDG kinetic model. The left compartment represents the vascular space for FDG, Ca. The middle compartment represents the extravascular space for FDG, Ce, and the right compartment represents the cellular space for phosphorylated FDG-6-Phosphate (FDG-6-P), Cm. The second and third compartments add up-to form the myocardial tissue compartment, C_T.

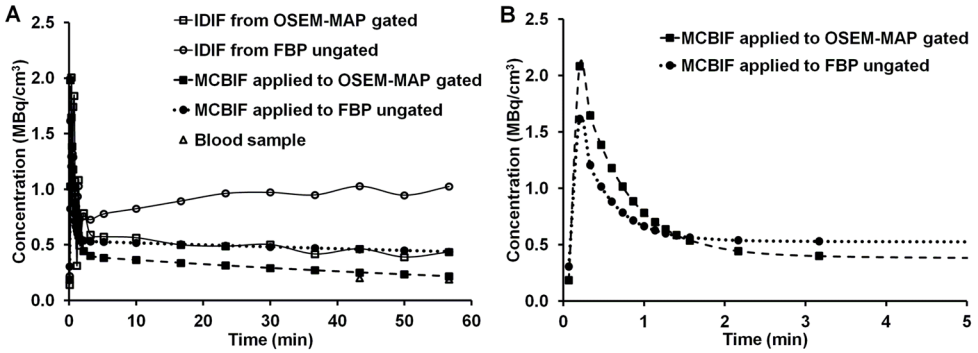

Figure 2.

Figure 2A. MCBIF estimation for the whole scan duration.. Representative IDIF's obtained from OSEM-MAP cardiac and respiratory gated images (line with open squares) and from FBP un-gated images (line with open circles) with attenuation correction. MCBIF applied to IDIF from the former (line with solid squares) and the latter (line with solid circles) are also shown in the figure. The venous blood samples at around 43 and 56 minutes are shown for comparison (open triangles). MCBIF applied to the IDIF obtained from high resolution gated images, correctly accounts for the wash-out dynamics of FDG from the blood, when compared to the late venous blood samples. **2B. MCBIF estimation during the first 5 minutes of the scan.** The scan indicates improved PV recovery when applied to IDIF obtained from OSEM-MAP gated images as compared to that obtained from un-gated FBP images.

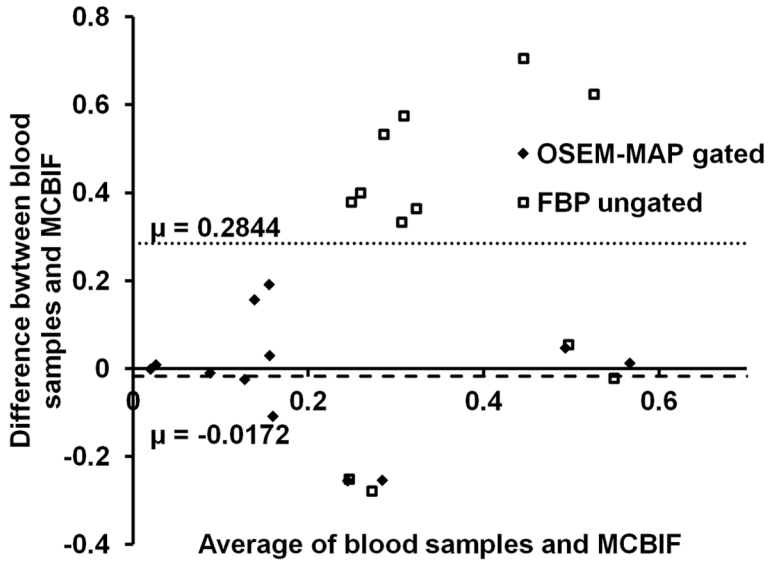

Figure 3. Residual plot

MCBIF applied to high resolution gated images, when compared to the 2 late venous blood samples revealed an average difference of 0.017 MBq/cc in n=6 control mice. The precision (standard deviation of differences) was 0.13 MBq/cc. The figure also shows the analysis obtained from FBP un-gated images. The plot indicated an average difference and precision to be 0.28 MBq/cc and 0.33 MBq/cc respectively obtained from the FBP un-gated data sets. The residual plot indicates the quantitative accuracy and repetitive behavior of the MCBIF applied to OSEM-MAP gated images.

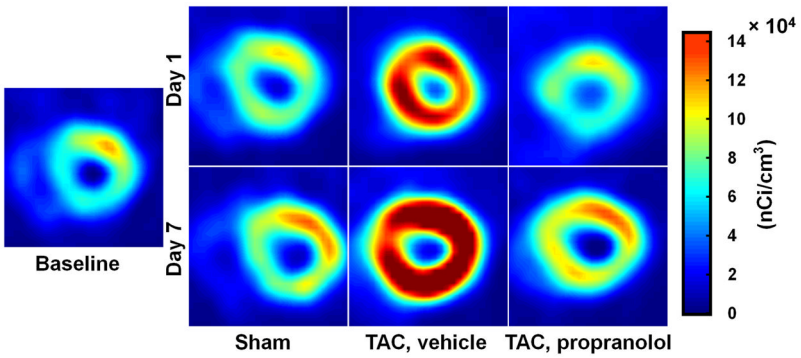

Figure 4. Gated transverse PET images *in vivo*

End-diastolic transverse PET images at the last time bin for sham, TAC, and TAC mice treated with propranolol at baseline, day 1 and day 7 post surgery are shown in this figure. All scans are from the same animals. The images indicate an enlargement in the LV cavity in the TAC mice over a period of 7 days. The images also show an increase in FDG uptake in the TAC mice starting at day 1 indicative of the metabolic adaptation in pressure overload LVH.

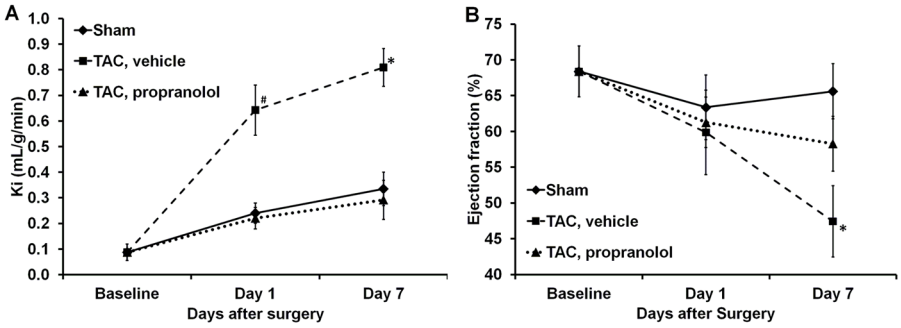

Figure 5.

Figure 5A. Measured rates of myocardial FDG uptake *in vivo*.. Ki (ml/g/min) for the mice in sham (n=5), TAC, vehicle (n=5) and TAC, propranolol (n=6) mice are shown in this figure. The figure shows increased myocardial FDG uptake at day 1 post TAC surgery by 580% indicating an adaptive response to stress. Ki increased further on day 7 in the TAC mice, while the TAC mice treated with propranolol exhibited attenuated rate of myocardial FDG uptake over the 7 days period. The metabolic changes in the TAC mice treated with propranolol were comparable to the shams. All values are mean ± SEM. *, #$p<0.05$ vs BSL, TAC treated with propranolol and sham groups.

5B. Measured LVEF from dynamic gated PET images *in vivo*. The plot indicates an insignificant drop in function in the TAC mice on day 1. On day 7 the function dropped by 24% in the TAC mice while there is an insignificant drop in function in the TAC mice treated with propranolol. The shams indicate no significant change in function over the 7 days period. All values are mean ± SEM. *$p<0.05$ vs BSL, TAC treated with propranolol and sham groups.

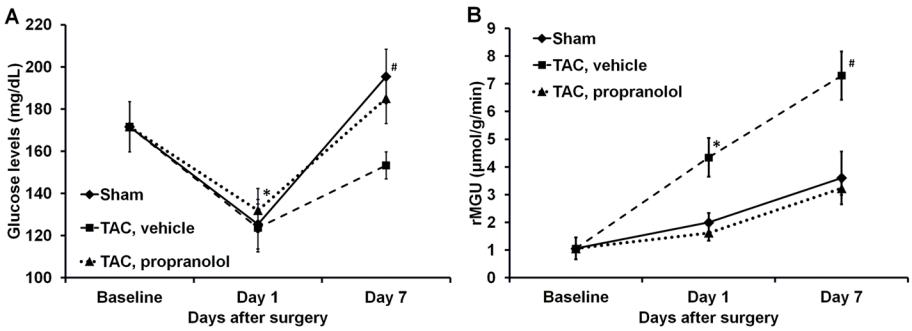

Figure 6.

Figure 6A. Blood glucose levels. The plot shows the average blood glucose levels measured at each time point for the sham, TAC and the TAC mice treated with propranolol. All the values are mean ± SEM. *p<0.05 vs BSL and day 1. #p<0.05 vs TAC at day 7. **6B. Rate of myocardial glucose utilization**. rMGU was measured at each time point for the sham, TAC and TAC mice treated with propranolol. All the values are mean ± SEM.*p<0.05 vs BSL, day 1, TAC treated with propranolol and sham groups. #p<0.05 vs BSL, TAC treated with propranolol and sham groups.

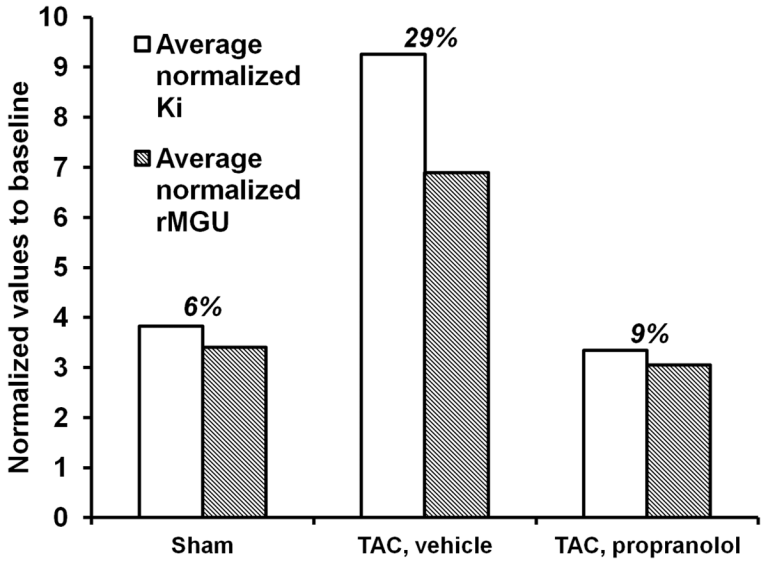

Figure 7. Comparison between Ki and rMGU measured *in vivo* at day 7

The rate of myocardial glucose utilization (rMGU) did not increase linearly with Ki. rMGU increased at a much slower rate than Ki, resulting in a mismatch of 29% between Ki and rMGU in the TAC mice. Treatment with propranolol reduced the mismatch to 9% and rescued cardiac function.